THE JOURNAL OF BIOLOGICAL CHEMISTRY
Vol. 278, No. 9, Issue of February 28, pp. 7381–7389, 2003
Printed in U.S.A.

Spectroscopic Characterization of the Electronic Changes in the Active Site of *Streptomyces antibioticus* Tyrosinase upon Binding of Transition State Analogue Inhibitors*

Received for publication, September 27, 2002, and in revised form, November 22, 2002
Published, JBC Papers in Press, December 6, 2002, DOI 10.1074/jbc.M206394200

Luigi Bubacco‡, Maurice van Gastel§, Edgar J. J. Groenen§, Erik Vijgenboom¶, and Gerard W. Canters¶‖

From the ‡Department of Biology, University of Padova, Viale G. Colombo 3, 35121, Padova, Italy, the §Department of Molecular Physics, Huygens Laboratory, Leiden University, P. O. Box 9504, 2300 RA Leiden, The Netherlands, and the ¶Leiden Institute of Chemistry, Gorlaeus Laboratories, Leiden University, P. O. Box 9502, 2300 RA Leiden, The Netherlands

The dinuclear copper enzyme tyrosinase (Ty) from genetically engineered *Streptomyces antibioticus* has been investigated in its paramagnetic half-met form [Cu(I)-Cu(II)]. The cw EPR, pulsed EPR, and hyperfine sublevel correlation spectroscopy (HYSCORE) experiments on the half-met-Ty and on its complexes with three different types of competitive inhibitor are reported. The first type includes *p*-nitrophenol, a very poor substrate for the monooxygenase activity of Ty. The second type comprises hydroxyquinones, such as kojic acid and L-mimosine, and the third type of inhibitor is represented by toluic acid. The electronic and structural differences of the half-met-Ty form induced at the cupric site by the different inhibitors have been determined. Probes of structural effects are the hyperfine coupling constants of the non coordinating Nδ histidyl nitrogens. By using the available crystal structures of hemocyanin as a template in combination with the spectroscopic results, a structural model for the active site of half-met-Ty is obtained and a model for the binding modes of both mono- and diphenols could be proposed.

The reaction mechanism of the binuclear copper enzyme tyrosinase (Ty)[1] (EC 1.14.18.1) is far from completely understood. Like catechol oxidase and the respiratory pigment hemocyanin (Hc), tyrosinase contains a so-called "type-3 copper" active site (1). Despite the wide distribution of Ty in nature, from bacteria to man, no crystal structure of the enzyme is available to date. It is current practice to use the crystal structures of other members of the type-3 copper protein family as structural models for Ty. These are the deoxygenated form of *Panulirus interruptus* Hc (2, 3), the deoxy and oxy forms of subunit II from *Limulus polyphemus* Hc (4–6), the oxy form of the odg domain of *Octopus dofleini* Hc (7) and, recently, the deoxy, met, and inhibitor-bound forms of the *Ipomoea batatas* catechol oxidase (8). The common structural theme of the type-3 active site in all crystallized proteins is the presence of six conserved histidine ligands that, three by three, co-ordinate the two copper ions through their Nε nitrogens. Despite the lack of a three-dimensional structure this structural theme could also be identified in *Streptomyces antibioticus* Ty in the oxidized [Cu(II)-Cu(II)] state by paramagnetic ^{1}H NMR (9). In that study, the protein was found to exhibit a well resolved paramagnetic spectrum despite its size (30 kDa), and the protein ligands to the binuclear copper site were identified as six Nε nitrogens. The other common structural feature of type-3 sites is the binding mode of molecular oxygen to the deoxy form [Cu(I)-Cu(I)], which in all cases results in a μ-η^2:η^2 peroxide-bound dicupric site. The spectroscopic properties typical for the binuclear cupric μ-η^2:η^2 peroxide complex have been described for the oxygenated forms of all proteins of this family (1).

The proteins can be distinguished according to their activity. Hcs reversibly bind oxygen under physiological conditions. They exhibit no enzymatic activity except for a very small catecholase activity for Hcs deriving from one of the two phyla in which Hcs have been detected, *i.e.* the molluscs (10) (the other one being the arthropods). Catechol oxidases oxidize catechols to *o*-quinones, but only the Tys can catalyze the monooxygenation of monophenols to *o*-diphenols (catechols) as well as the oxidation of diphenols to *o*-quinones with molecular oxygen as a co-substrate. Direct structural information on Tys would be helpful for proposing a model for the molecular mechanism of its complex enzymatic activity, but the structural investigation of Tys is hindered by two issues, the very low level of expression of these enzymes in natural systems and their limited accessibility to common spectroscopic techniques. In the present study the first issue was solved by the use of an overexpression system for bacterial Ty from *S. antibioticus*, which allowed the production of milligram amounts of Ty. The second issue was addressed by the generation of a paramagnetic active site through partial reduction of the met form. The partial reduction of the EPR silent met-Ty to the half-met [Cu(I)-Cu(II)] form has been previously described for *Neurospora crassa* Ty (11), and on the basis of cw EPR spectroscopy of this derivative and its inhibitor-bound complexes, a reaction mechanism was proposed whereby the hydroxy group of the incoming phenol binds at an axial coordination position of one copper of [Cu(II)-O_2^{2-}-Cu(II)] oxy-Ty and subsequently undergoes a Berry-pseudorotation to an equatorial position (12, 13). Later on these proposals were elaborated in light of further experimental evidence. A survey of these models has been recently presented (14). It emerges, however, that questions remain open with regard to the mode of binding of the phenolic substrates to the copper and the sequence of intermediary steps in the enzymatic reaction (14).

* The costs of publication of this article were defrayed in part by the payment of page charges. This article must therefore be hereby marked "*advertisement*" in accordance with 18 U.S.C. Section 1734 solely to indicate this fact.

‖ To whom correspondence should be addressed. Tel.: 31-71-527-4256; Fax: 31-71-527-4349; E-mail: canters@chem.leidenuniv.nl.

[1] The abbreviations used are: Ty(s), tyrosinase(s); Hc(s), hemocyanin(s); HYSCORE, hyperfine sublevel correlation spectroscopy; ESEEM, electron spin echo envelope modulation; cw, continuous wave.

To shed more light on these questions, we have performed cw EPR, pulsed EPR, and hyperfine sublevel correlation spectroscopy (HYSCORE) experiments on half-met-tyrosinase from *S. antibioticus* and on its complexes with three types of competitive inhibitor. The first type is represented by *p*-nitrophenol, a very poor substrate for the monooxygenase activity of Ty. On the time scale of the sample preparation it forms a stable complex with half-met-Ty. The second type of inhibitor is formed by hydroxyquinones such as kojic acid and L-mimosine. These molecules can be considered intermediate state analogues since they exhibit a structural analogy to the quinone reaction products as well as to the diphenolic substrates while occurring in an oxidation state that is not suitable for reaction. The third type of inhibitor is represented by toluic acid. This is a competitive inhibitor and a substrate analogue in which the carboxylate group, which is conjugated to the aromatic ring, is expected to bind to the cupric center of half-met-Ty. The aim of the present work is to characterize the half-met-Ty form and to explore the electronic and structural differences brought about by binding of the inhibitors. Probes for such structural effects are the hyperfine coupling constants from the non-coordinating histidyl nitrogens of half-met-Ty. These have been obtained from simulations of the electron spin echo envelope modulation (ESEEM) spectra and HYSCORE spectra of half-met-Ty (15).

MATERIALS AND METHODS

The host for the expression of tyrosinase, *S. antibioticus* (LMD 86.18), was obtained from the collection of the Kluyver Laboratory of the Delft Technical University, The Netherlands. The plasmid that contains the tyrosinase operon (*melC1* and *melC2*) and the thiostrepton resistance marker was kindly provided by Prof. E. Katz (16). Tyrosinase was purified following the procedure described previously (17). The purified protein was obtained as a mixture of [Cu(II)-OH^--Cu(II)] met-Ty (~90%), [Cu(II)-O_2^{2-}-Cu(II)] oxy-Ty, and [Cu(I)-Cu(I)] deoxy-Ty. After concentration the charge-transfer band at 350 nm, characteristic for the oxy form of the protein (18), was absent. The met-Ty was divided into aliquots and stored in 18% (w/w) ethylene glycol at −20 °C. The protein concentrations of the solutions used in the EPR experiments were determined by measurement of the optical absorption at 280 nm using a molar extinction coefficient of 82.1 mM^{-1} cm^{-1} (19).

The selective reduction of one of the two coppers in the active site was carried out by mixing 1 ml of 0.5 mM met-Ty in 20 mM phosphate buffer at pH 6.8 with $NaNO_2$ and ascorbic acid buffered solutions to a final concentration of 40 mM and 4 mM, respectively (modified from Refs. 11 and 12). The formation of the enzymatically inactive half-met-Ty was followed by monitoring the specific activity of the protein solution with respect to the conversion of DOPA (as described in Ref. 20). When no further decrease of activity was detected, the protein solution, which has a pale green color, was purified with a desalting column (Sephadex G-25), which was previously equilibrated with 20 mM phosphate buffer at pH 6.8. The residual activity was less than 4% of the starting activity indicating less than 4% of the Ty being present in the red, oxy, and met form. The latter forms of Ty are EPR-inactive, anyway. The half-met-Ty solution was then concentrated in an Amicon® ultrafiltration system to a final concentration of 0.7 mM.

The complexes of half-met-Ty with inhibitor were obtained by addition of small aliquots of buffered inhibitor solution at a concentration of 20 mM to achieve a final concentration of 2 mM. After addition of the inhibitor, the samples were frozen immediately by immersion in liquid nitrogen.

The 95-GHz (W-band) ESE-detected EPR experiment for a frozen solution of half-met-tyrosinase (T = 1.2 K) was performed on a home-built spectrometer described in Ref. 21 except for the microwave bridge, which was replaced by a bridge from the Department of Microwave Equipments for Millimeter Waveband ESR Spectroscopy in Donetsk, Ukraine. Microwave pulses of 100 and 150 ns were used, and the time between the microwave pulses was 300 ns. The repetition rate of the pulse sequence was 66 Hz. The 9-GHz (X-band) continuous wave EPR experiments were performed on a Bruker ESP380E EPR spectrometer. The microwave frequency was 9.40 GHz for half-met-Ty, half-met-Ty with L-mimosine, half-met-Ty with toluic acid, and half-met-Ty with kojic acid and 8.95 GHz for half-met-Ty with *p*-nitrophenol. The modulation field was 0.5 millitesla, and the modulation frequency 100 kHz. To verify that no copper was removed from the active site of the protein by the excess of inhibitors, the cw EPR spectra of a 2-mM $CuSO_4$ solution plus inhibitor at the same concentration as the Ty sample were collected. These bear no resemblance to the spectra presented here for the Ty inhibitor complexes.

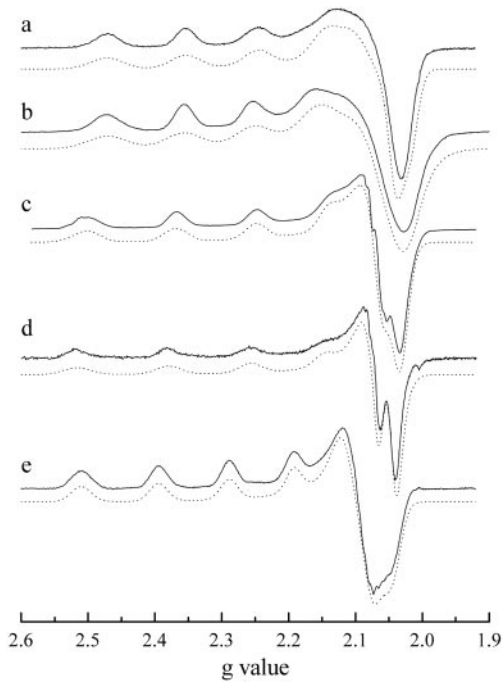

FIG. 1. **X-band cw EPR spectra and simulations of half-met-Ty and its complexes with substrate analogue inhibitors.** *a*, half-met-Ty; *b*, half-met-Ty with *p*-nitrophenol; *c*, half-met-Ty with L-mimosine; *d*, half-met-Ty with kojic acid; *e*, half-met-Ty with toluic acid. Spectrum (*e*) has been corrected for the presence of a small signal of half-met-Ty.

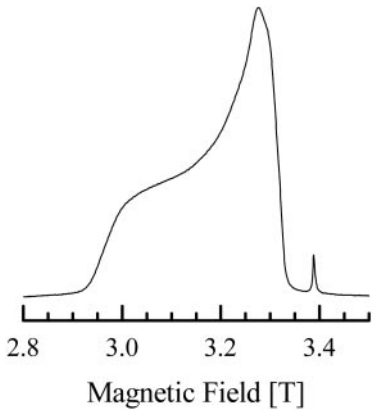

FIG. 2. **W-band ESE-detected EPR spectrum of half-met-Ty.** The sharp signal at about 3.4 T corresponds to a carbon radical (g = 2.0028) present in the capillary tube.

The ESEEM experiments were performed with a 3-pulse sequence in which the microwave pulses had a length of 16 ns. The microwave frequency was 9.74 GHz for half-met-Ty, 9.75 GHz for half-met-Ty with L-mimosine, and 9.73 GHz for half-met-Ty with *p*-nitrophenol. The time T between the second and third microwave pulse was scanned, starting at 56 ns and incremented with steps of 8 ns. In total, 2048 data points were acquired. Two series of modulation patterns were recorded. In the first series, in which the time τ between the first and second microwave pulse was fixed at 120 ns for half-met-Ty and 144 ns for half-met-Ty with *p*-nitrophenol or L-mimosine, the modulation patterns were measured at different magnetic field settings. In the second series the modulation patterns were measured at different τ values and the magnetic field was fixed to the position of maximum absorption in the ESE-detected EPR spectrum (335 millitesla for half-met-tyrosinase, 332.5 millitesla for half-met-tyrosinase with *p*-nitrophenol, and 337.5 millitesla half-met-tyrosinase with L-mimosine). The background of the

TABLE I

g values and copper hyperfine coupling constants (MHz) obtained by simulation of the cw EPR spectra of half-met-Ty and its inhibitor complexes (except for the g values for half-met-Ty, which stem from simulations of the ESE-detected EPR spectra at 9 and 95 GHz)

In the cw EPR spectrum of the half-met-Ty with L-mimosine a superhyperfine interaction in the perpendicular region is present with a splitting of about 40 MHz.

	Half-met-Ty[a]	Half-met-Ty with *p*-nitrophenol	Half-met-Ty with L-mimosine	Half-met-Ty with kojic acid	Half-met-Ty with toluic acid
g_{zz}	2.298	2.298	2.305	2.316	2.332
g_{yy}[b]	2.077	2.082	2.081	2.074	2.124
g_{xx}[b]	2.059	2.054	2.062	2.072	2.056
A_{zz}	442	452	489	496	420
A_{yy}[b]	96	20	20	10	90
A_{xx}[b]	25	40	20	20	22

[a] The values for other half-met derivatives are: *N. crassa* Ty (g_{zz} = 2.296, A_{zz} = 393 MHz) (11), *Octopus vulgaris* hemocyanin (g_{zz} = 2.294, A_{zz} = 425 MHz) (31).

[b] A precise evaluation of these parameters is hindered by the broad lineshape of the spectra in this region.

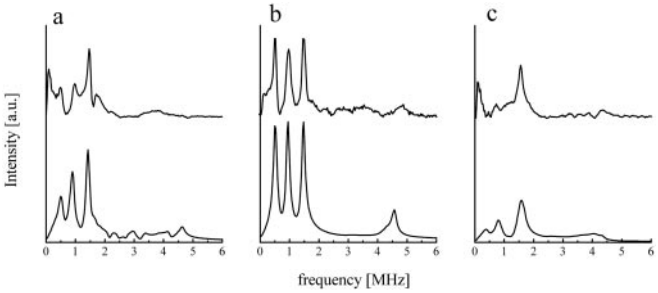

FIG. 3. **Experimental (*upper traces*) and simulated (*lower traces*) X-band ESEEM spectra of half-met-Ty (*a*), half-met-Ty with *p*-nitrophenol (*b*), and half-met-Ty with L-mimosine (*c*).** The magnetic field setting is 335 millitesla for *a*, 332.5 millitesla for *b*, and 337.5 millitesla for *c*. The time τ is 120 ns for *a* and 144 ns for *b* and *c*.

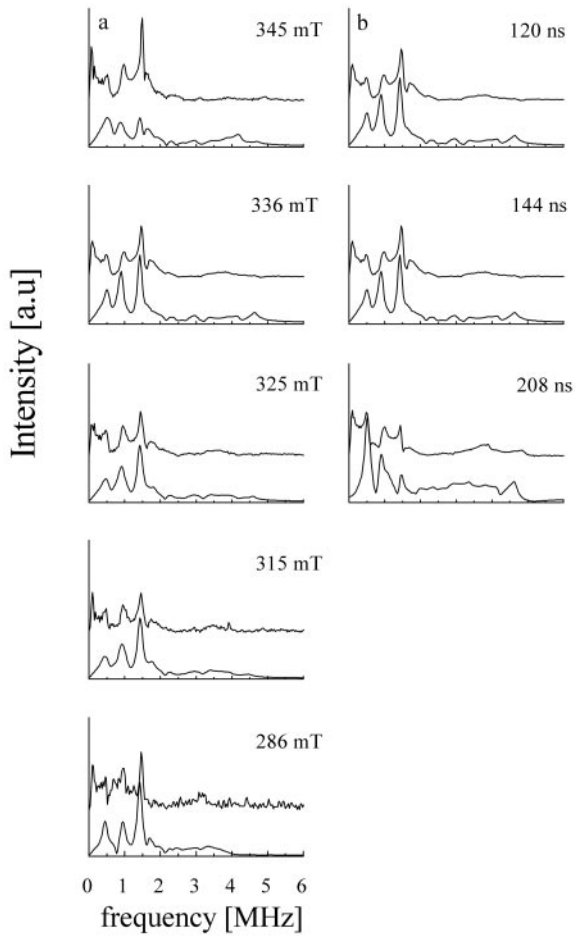

FIG. 4. **Experimental (*upper traces*) and simulated (*underneath each experimental trace*) X-band ESEEM spectra of half-met-Ty.** In *a* the time τ was kept fixed at 144 ns, and in *b* the magnetic field was fixed at 336 millitesla.

modulation patterns was removed by fitting and subsequently subtracting a Gaussian function. No window function was used. The data were zero-filled to 4096 data points and subsequently Fourier-transformed to obtain magnitude ESEEM spectra.

The HYSCORE experiments were performed with a $\pi/2$-τ-$\pi/2$-T_2-π-T_1-$\pi/2$ microwave pulse sequence with $\pi/2$ pulses of 16 ns and a π pulse of 24 ns. In a HYSCORE spectrum, cross-peaks from nitrogens are expected at ($\pm\nu_Q$, $\pm\nu_{DQ}$) and ($\pm\nu_{DQ}$, $\pm\nu_Q$), where the first coordinate represents the frequency related to T_1 and the second coordinate the frequency related to T_2. The symbol ν_Q corresponds to one of the three quadrupole frequencies of the cancelled M_S manifold and the symbol ν_{DQ} to the so-called $\Delta M_I = 2$ or double-quantum transition of the non-cancelled M_S manifold. For half-met-tyrosinase the magnetic field setting was 335 millitesla, for half-met-Ty with nitrophenol it was 332.5 millitesla, and for half-met-Ty with L-mimosine it was 337.5 millitesla. The microwave frequency was the same as for the ESEEM experiments. The time τ between the first and second microwave pulse was fixed at 192 ns. In total 512 × 256 data points were acquired in the T_1 and T_2 direction, respectively. Starting times of T_1 and T_2 were 168 and 136 ns, respectively, and the time increments were 16 ns for both. The background of the resulting two-dimensional modulation patterns was subtracted by a quadratic fit first to the slices at fixed T_2 and then to the slices at fixed T_1. Apodization was performed with a Hamming window function. The data were zero-filled to 1024 × 512 points and transformed into the frequency domain by a two-dimensional Fourier transformation. The spectra are represented as magnitude contour spectra.

Simulations of the cw EPR spectra have been carried out with the software EPR (22). According to the procedure outlined and discussed in Ref. 23, the ESEEM spectra were simulated as follows. The expectation value of the electron spin operator $\vec{S}$ was calculated from the Hamiltonian of the electron Zeeman interaction and the copper hyperfine interaction, given by

$$H_e = \beta_e \vec{B}_0 \cdot \vec{\vec{g}} \cdot \vec{S} + S_z A_{zz}^{Cu} M_I^{Cu} \qquad \text{(Eq. 1)}$$

where β_e is the Bohr magneton, $\vec{B}_0$ the magnetic field, $\vec{\vec{g}}$ the g tensor, A_{zz}^{Cu} the copper hyperfine interaction along the *z* principal axis of the g tensor, and M_I^{Cu} the magnetic quantum number of the nuclear spin of copper. Subsequently, the expectation value was inserted into the nuclear spin Hamiltonian for nitrogen, which consists of the nuclear Zeeman interaction, the nitrogen hyperfine interaction, and the following quadrupole interaction.

$$H_n = -g_N \beta_n \vec{B}_0 \cdot \vec{I} + \langle \vec{S} \rangle_{\alpha,\beta} \cdot \vec{\vec{A}} \cdot \vec{I} + \vec{I} \cdot \vec{\vec{Q}} \cdot \vec{I} \qquad \text{(Eq. 2)}$$

In this equation g_N is the g value of nitrogen, β_n the nuclear magneton, $\vec{\vec{A}}$ the hyperfine tensor, and $\vec{\vec{Q}}$ the quadrupole tensor. From the eigenvalues and eigenvectors of the nuclear spin Hamiltonian, the contribution of a single nitrogen to the modulation function was calculated according to the formula derived by Mims (24, 25). These steps were repeated for the nitrogens that contribute to the spectrum, for the values of M_I^{Cu}, and for the α and the β values of the electron spin using the appropriate product formula (23). Finally, to simulate a spectrum of a frozen solution, about 3100 directions of $\vec{B}_0$ are considered. The decay of the echo and the modulations and the dead time of

the spectrometer were taken into account as described in Ref. 23 with time constants of 400 μs, 4 μs, and 298 ns, respectively.

The principal values of the g tensor are called g_{xx}, g_{yy}, and g_{zz}, and the principal axes are called x, y, and z. For each nitrogen, the quadrupole tensor is specified by principal values $Q_{x'x'}$, $Q_{y'y'}$, and $Q_{z'z'}$ and principal axes x', y', and z', and the hyperfine tensor is specified by principal values $A_{x''x''}$, $A_{y''y''}$, and $A_{z''z''}$ and principal axes x'', y'', and z''. The principal values of the quadrupole tensor are related to the parameters e^2qQ and η that describe the electric field gradient at the nitrogen according to $Q_{x'x'} = e^2qQ(\eta - 1)/4$, $Q_{y'y'} = -e^2qQ(\eta + 1)/4$ and $Q_{z'z'} = e^2qQ/2$.

RESULTS

cw and ESE-detected EPR—The continuous wave EPR spectra at 9 GHz of frozen solutions of *S. antibioticus* half-met-tyrosinase and half-met-Ty with the inhibitors *p*-nitrophenol, L-mimosine, kojic acid, and toluic acid are presented in Fig. 1. To obtain accurate g values for half-met-Ty, an ESE-detected EPR spectrum was recorded at 95 GHz (Fig. 2), which provided for superior g value resolution. Simulations of the cw EPR spectra are included in Fig. 1, and the g values (g_{xx}, g_{yy}, g_{zz}) and copper hyperfine values (A_{xx}, A_{yy}, A_{zz}) of the simulations are given in Table I.

The spectra are characterized by large g_{zz} and A_{zz} values, consistent with a singly occupied molecular orbital in the ground state of $d_{x^2-y^2}$ or d_{xy} character on copper (26). For half-met-Ty, the g values obtained from independent simulation of the spectra at 9 and 95 GHz are consistent with those reported previously for the half-met derivative of *N. crassa* Ty (11, 12). The g_{zz} value amounts to 2.298 and the rhombicity ($g_{yy} - g_{xx}$) to 0.018. The spectrum of half-met-Ty with *p*-nitrophenol is similar to that of half-met-Ty. Only around g = 2.1 do the spectra differ. When L-mimosine binds, the cw EPR spectrum is characterized by larger g_{zz} and A_{zz} values. Superhyperfine structure becomes visible in the g_{xx}/g_{yy} region and on the copper hyperfine band at g = 2.5. For half-met-Ty with kojic acid, the g_{zz} and A_{zz} values become even larger. The complex of half-met-Ty with toluic acid is characterized by the largest g_{zz} and smallest A_{zz} value. It is clear that binding of the inhibitors investigated in this study results in significant changes in EPR parameters. As we are dealing here with competitive inhibitors they must bind at or close to the copper site. However, the fact that nitrophenol can also act as a substrate, albeit a very poor one (45), is diagnostic of binding to the copper. The only inhibitor/enzyme complex of a type-3 copper protein of which a structure has been reported in the literature is catechol oxidase (8), where the thiourea inhibitor binds directly to the copper site. Other (indirect) structural evidence on the binding mode of inhibitors relates to the release of a water molecule or an OH^- moiety from the first coordination shell of the paramagnetic copper in half-met-Ty upon inhibitor binding (23), making it likely that the leaving moiety is replaced by an oxygen of the inhibitor. For the met-form of Ty there has also been found direct evidence for coordination to the copper since the contact-shifted NMR signals of the inhibitors have been observed in the 600-MHz NMR spectra of the inhibitor/Ty complexes.[2] Taking all this evidence into account it appears that the simplest way to interpret the present data is to assume that the inhibitors directly bind to the copper.

ESEEM—In Fig. 3, three-pulse ESEEM spectra for frozen solutions of half-met-Ty, half-met-Ty with *p*-nitrophenol, and half-met-Ty with L-mimosine are presented, recorded at the magnetic field of maximum absorption in the ESE-detected EPR spectrum. The ESEEM spectrum of half-met-Ty (Fig. 3*a*) is characterized by three bands at about 0.5, 1.0, and 1.5 MHz and a broad and weak band around 4 MHz, typical for a remote (amino) nitrogen of a histidine that ligates to copper (27). An additional band is present at 1.7 MHz. For half-met-Ty with *p*-nitrophenol (Fig. 3*b*), the three bands at 0.5, 1.0, and 1.5 MHz become more pronounced compared with those for half-met-Ty. One band at 1.6 MHz dominates the ESEEM spectrum for half-met-Ty with L-mimosine (see Fig. 3*c*).

For each of these samples a series of ESEEM spectra were collected for different magnetic field settings and different values of the time τ between the first and second microwave pulses. For half-met-Ty a number of these are shown in Fig. 4. The frequencies of the bands below 2 MHz are almost independent of the value of the magnetic field, but their relative intensities vary. When the value of the time τ is changed, the relative intensities are affected more. For example, at τ = 120 ns or 144 ns, the band at 1.5 MHz dominates, and at τ = 208 ns,

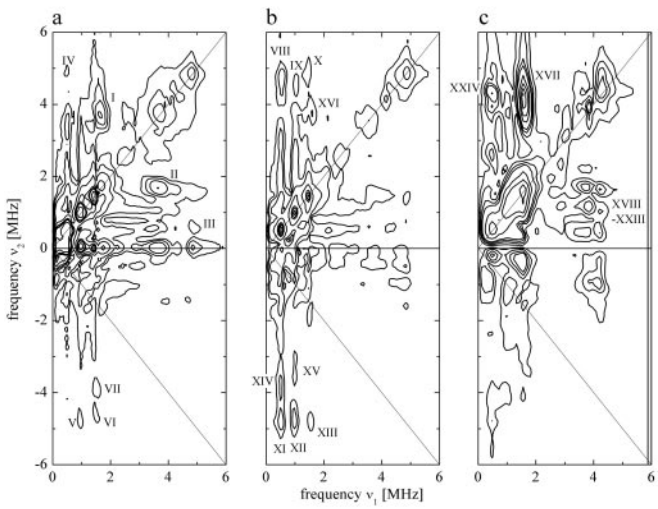

FIG. 5. **X-band HYSCORE spectra of half-met-Ty (*a*), half-met-Ty with *p*-nitrophenol (*b*), and half-met-Ty with L-mimosine (*c*).**

[2] L. Bubacco and G. W. Canters, unpublished results.

TABLE II

Frequencies (MHz) of the cross-peaks in the HYSCORE spectra of half-met-Ty, half-met-Ty with p-nitrophenol and half-met-Ty with L-mimosine

Half-met-Ty											
III	0.6	4.9	V	1.0	4.8	I	1.6	3.7	VII	1.5	3.9
IV	0.5	4.9	VI	1.5	4.6	II	1.7	3.7			
Half-met-Ty with *p*-nitrophenol											
VIII	0.5	4.7	XII	1.0	4.7	XIV	0.5	3.8			
IX	1.0	4.6	XIII	1.6	4.8	XV	1.0	3.3			
X	1.4	4.9				XVI	1.6	3.7			
XI	0.5	4.8									
Half-met-Ty with L-mimosine											
XVII	1.6	4.1	XXI	1.1	4.2						
XVIII	1.6	3.8	XXII	0.5	3.8						
XVIX	1.6	4.2	XXIII	0.5	4.2						
XX	1.1	3.8	XXIV	0.5	4.3						

this band is weaker than the one at 0.5 MHz. The intensities of the broad bands around 4 MHz also vary.

HYSCORE—Fig. 5*a* shows the HYSCORE spectrum of half-met-Ty, recorded at the field of maximum absorption in the ESE-detected EPR spectrum. On the diagonal, bands are visible at the same frequency as the bands in the corresponding ESEEM spectrum. For example, the three sharp bands appear at (ν_1, ν_2) = (0.5, 0.5), (1.0, 1.0), and (1.5, 1.5) MHz. Two strong cross-peaks, labeled I and II are visible at (1.7, 3.7) and (3.7, 1.7) MHz. Weak cross-peaks III-VI correlate 0.5, 1.0, and 1.5 MHz to about 4.8 MHz. The frequencies correlated by the cross-peaks are summarized in Table II. A more resolved pattern is observed in the HYSCORE spectrum of half-met-Ty with *p*-nitrophenol (Fig. 5*b*). Similar to the case of half-met-Ty, the bands on the diagonal correspond to the bands in the ESEEM spectrum. The frequencies of the sharp bands (0.5, 1.0, 1.5 MHz) are connected to about 4.8 MHz by the weak cross-peaks XI-XIII. The peak marked by XVI occurs at the same position as the one marked by I in the spectrum for half-met-Ty, but its intensity is smaller. The HYSCORE spectrum for half-met-Ty with L-mimosine is shown in Fig. 5*c*. The spectrum is dominated by cross-peak XVII at (1.6, 4.2) MHz. A cluster of six cross-peaks connects the frequencies 0.4, 1.2, and 1.6 MHz to 3.8 and 4.2 MHz. The frequencies 0.4 and 1.2 MHz are not resolved in the ESEEM spectrum.

DISCUSSION

cw EPR—The controlled oxidation of only one copper in the binuclear type-3 active site provides a sensitive paramagnetic probe for the investigation of the interaction between the metal ion and substrates or transition state analogue inhibitors. In this study *S. antibioticus* tyrosinase has been first purified from an overexpression system and then converted to the half-met form following the protocol described for *N. crassa* Ty (11, 12). The cw EPR spectra of the half-met derivative of bacterial tyrosinase are similar to those of the other half-met derivatives of type-3 sites (*cf.* Table I) suggesting that at least for the half-met derivative a substantial structural similarity exists within this "type" of active sites.

When competitive inhibitors are added to a solution of bacterial half-met-Ty, the g_{zz} value and copper hyperfine component A_{zz} are affected. As already mentioned in the Introduction, the inhibitors used can be divided into three types: monophenols (*p*-nitrophenol), hydroxyquinones (L-mimosine and kojic acid), and carboxylated substrates (toluic acid). When the paramagnetic properties are analyzed in terms of coordination number of the cupric copper, all complexes have large g_{zz} and A_{zz} values (*cf.* Table I). In Fig. 6, a Vänngård-Peisach-Blumberg plot (28) is shown in which in addition to the properties of the various half-met-Ty complexes also a number of four- and five-coordinate Cu(II) model complexes and copper proteins are included. Two different linear correlations between g_{zz} and A_{zz} values can be identified in the plot (Fig. 6*B*). It is known that coordination shells with the same number of ligands but of different composition may give rise to shifts in A and g values and so care must be exercised in drawing conclusions from the location of new points in such a diagram. We notice, however, that the points on the four-coordinate correlation line all derive from complexes with aromatic-like ligands and as such appear to lie on a single line. Half-met-Ty and half-met-Ty with *p*-nitrophenol are close to the line that corresponds to the four coordinate copper centers (only 3N1O complexes have been included in the plot), while half-met-Ty with L-mimosine or kojic acid is closer to the line for the five-coordinated model complexes (3N2O). Still close to the linear regression of five-coordinated model complexes but in a different region of the plot are the values referring to the toluic acid complex. It is therefore tentatively concluded that the cupric site of half-met-Ty is four-coordinated. It remains four-coordinated when a monophenol binds and becomes five-coordinated when a hydroxyquinone or toluic acid binds.

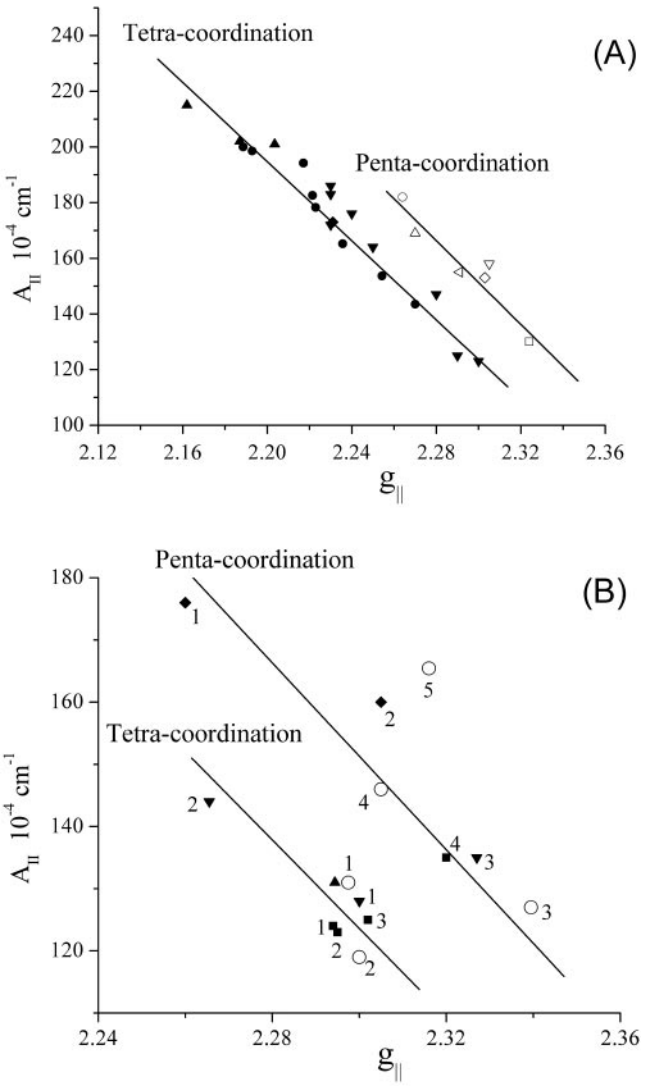

FIG. 6. **Vänngård-Peisach-Blumberg plot (28) of the $A_{||}$ *versus* $g_{||}$ values for a series of tetra (4N, 3N1O, and 2N2O)- and penta (3N2O)-coordinated copper complexes (*A*) and copper proteins (*B*).** *A*, *tetra-coordinated* copper complexes of known crystal structure: ▲, three complexes, Nanomura and co-workers (38); ▼, 10 complexes, Rosenberg *et al.* (37); ●, eight complexes, Sakaguchi and Addison (39); ♦, Bhalla *et al.* (40). Penta-coordinated copper complexes of known crystal structure: ○, Wilcox *et al.* (12); ◇, Barta and Mathur (41); △, Cu(II) of the octa-repeat domain of prion protein (42); ▽, Cu(II)-insuline (43); ◭, imidazole adducts of Cu(II) valproate (44); ■, Cu(II) complex of diethylene triamine and valproic acid.[4] *B*, type-3 binuclear copper proteins: ○, half-met-Ty from *S. antibioticus*: 1) native, 2) plus nitrotyrosine, 3) plus L-mimosine, 4) plus toluic acid, 5) plus kojic acid; ▲, half-met-Ty from *N. crassa* (11); ■, half-met-Hc from 1) *Carcinus maenas* (31), 2) *Octopus vulgaris* (31), 3) *L. poliphemus* (31), 4) mononuclear Hc of *Carcinus aestuarii* (34). *Mononuclear* copper proteins: ▼, 1) nitrite reductase (35), 2) superoxide dismutase (36), and 3) carboxypeptidase A (37). ♦, 1) and 2) C112H/H117G double mutants of azurin (L. J. C. Jeuken and G. W. Canters, unpublished results). The *continuous lines* represent linear regressions for the tetra-coordinated and penta-coordinated copper centers obtained from Fig. 6*A*.

ESEEM and HYSCORE—More information about the coupling of the histidines to copper is obtained from the HYSCORE spectra and simulations of the ESEEM spectra. At X-band, the hyperfine interaction and the nuclear Zeeman interaction of the remote nitrogens of the histidines are about equal in mag-

TABLE III

Nitrogen hyperfine and quadrupole tensors obtained from simulation of the X-band ESEEM spectra for half-met-Ty, half-met-Ty with p-nitrophenol, and half-met-Ty with L-mimosine

The principal values of the hyperfine tensor and the parameter e^2qQ are in MHz.

	A_{iso}	$A_{x''x''}$	$A_{y''y''}$	$A_{z''z''}$		x	y	z	e^2qQ	η		x	y	z
							Half-met-Ty							
His-364	1.80	2.40	1.30	1.70	x″	−0.125	0.970	0.207	1.50	0.65	x′	−0.391	0.671	0.630
					y″	−0.444	−0.241	0.863			y′	−0.273	−0.738	0.617
					z″	0.887	0.016	0.461			z′	0.879	0.069	0.472
His-324	1.35	1.85	1.05	1.15	x″	0.911	−0.367	0.187	1.70	0.60	x′	0.387	−0.863	0.323
					y″	−0.380	−0.924	0.038			y′	−0.851	−0.470	−0.236
					z″	0.159	−0.106	−0.982			z′	0.356	−0.184	−0.916
							Half-met-Ty with *p*-nitrophenol							
His-364	2.10	2.30	1.90	2.10	x″	−0.125	0.970	0.207	1.60	0.65	x′	−0.391	0.671	0.630
					y″	−0.444	−0.241	0.863			y′	−0.273	−0.738	0.617
					z″	0.887	0.016	0.461			z′	0.879	0.069	0.472
							Half-met-Ty with L-mimosine							
His-364	1.50	2.03	1.18	1.30	x″	−0.330	0.720	0.610	1.60	0.65	x′	−0.391	0.671	0.630
					y″	−0.322	−0.694	0.644			y′	−0.273	−0.738	0.617
					z″	0.887	0.016	0.461			z′	0.879	0.069	0.472

nitude. In one of the M_S manifolds, these two interactions cancel and the frequency of the three nuclear transitions is determined by the quadrupole interaction (29). Three relatively sharp bands are expected from this manifold, usually between 0 and 2 MHz. The other M_S manifold gives rise to one band around 4 MHz that corresponds to the $\Delta M_I = 2$ transition. To retrieve information about the coupling of the histidines to copper, we use the cross-peaks in the HYSCORE spectra to identify the four frequencies that stem from one nitrogen. Once the frequencies have been identified, simulation of a large number of ESEEM spectra yields quantitative information about the hyperfine and quadrupole interaction for each nitrogen.

In a HYSCORE spectrum, cross-peaks are expected at ($\pm\nu_Q$, $\pm\nu_{DQ}$) and ($\pm\nu_{DQ}$, $\pm\nu_Q$), where ν_{DQ} is the $\Delta M_I = 2$ transition and ν_Q one of the three bands below 2 MHz. The cross-peaks III–VI in the HYSCORE spectrum of half-met-Ty (Fig. 5*a*) correlate the frequencies 0.5, 1.0, and 1.5 MHz to about 4.8 MHz (*cf.* Table II). These frequencies therefore stem from one remote nitrogen of a histidine. Cross-peaks I, II, and VII correlate 1.6 MHz to about 3.8 MHz and indicate the contribution of a nitrogen from a second histidine. Given the relatively large intensity of cross-peaks I and II, both 1.6 and 3.8 MHz correspond to fundamental frequencies of the second nitrogen. Sum and difference frequencies are not observed. When *p*-nitrophenol binds (Fig. 5*b*), the frequencies of the bands of the first nitrogen, correlated by cross-peaks VIII–XIII, are virtually unchanged, as was the case for the ESEEM spectra. The contribution of the second nitrogen has become considerably less pronounced, as indicated by the relatively low intensity of peak XVI compared with I. Cross-peaks XIV, XV and XVI are tentatively assigned to the second nitrogen, whose frequencies thereby become 0.5, 1.0, 1.6, and 3.7 MHz. For half-met-Ty with L-mimosine (Fig. 5*c*), more drastic changes occur as regards the intensity distribution. Cross-peaks XVII–XXIV correlate 0.5, 1.1, and 1.6 MHz to $\Delta M_I = 2$ frequencies at 3.8 and 4.2 MHz. It is unclear whether the frequencies 3.8 and 4.2 MHz belong to one nitrogen.

The simulations of the ESEEM spectra of half-met-Ty and its inhibitor complexes are included in Figs. 3 and 4 underneath the experimental spectra. Based on the HYSCORE data, the simulations for half-met-Ty include two nitrogens. For half-met-Ty with *p*-nitrophenol, only the dominant nitrogen is considered in the simulation as the contribution of the second nitrogen is minor. For half-met-Ty with L-mimosine no direct evidence for a second nitrogen is present in the HYSCORE spectrum and one nitrogen is included in the simulation. In the ESEEM simulations, the hyperfine and quadrupole tensors for each nitrogen enter as parameters. In principle, this would mean 11 free parameters for each nitrogen, six for the hyperfine tensor and five for the (traceless) quadrupole tensor. Fortunately, this number can be limited considerably. From nuclear quadrupole resonance studies (32), it is known that the principal axes of the quadrupole tensor of the remote histidine nitrogens are (within 10 °) directed as follows: one axis along the N–H bond (x'), the second perpendicular to the imidazole plane (z'), and the third perpendicular to the first two (y'). The two parameters e^2qQ and η that specify the principal values of the quadrupole tensor are read from the frequencies of the three quadrupole transitions observed in the ESEEM spectra (initial values of 1.5 and 0.6 MHz, respectively). The directions of the principal axes of the hyperfine tensor are based on those found for the remote histidine nitrogens in the blue-copper site of *P. aeruginosa* azurin (30), one axis along the Cu-Nδ direction (x''), one perpendicular to the imidazole plane and subsequently orthogonalised to the first (z''), and the third orthogonal to the first two (y''). To perform the simulations structural input is needed for the active site. Because at present no crystallographic data exists for tyrosinase, we used the data published for subunit II from *L. polyphemus* hemocyanin (PDB ID 1LL1) (4, 5), the amino acid sequence and the spectroscopic properties of which are similar to those of Ty. Initial guesses for the principal values of the hyperfine tensors are taken from an ESEEM study of green half-met hemocyanin (31). The simulations are performed using the principal axes system of the g tensor as a reference system. Because of the $d_{x^2-y^2}$ nature of the singly occupied molecular orbital and the near-axial g tensor we chose the z-axis of the g tensor perpendicular to the plane spanned by the bonds connecting the copper with Nϵs of histidines 324 and 364 (amino acid numbering from *L. polyphemus* sequence).[3]

The simulations performed with the initial parameter set already qualitatively reproduce the bands in the spectrum and their relative intensity, provided that the remote nitrogen of histidine 364 is assigned the largest hyperfine coupling from

[3] An analogous calculation was carried out using the crystal structure of the odg subunit of *O. dofleinii* Hc kindly provided by M. E. Cuff (7). This protein, the overall sequence of which is closer to that of bacterial Ty than that of *L. polyphemus* Hc, provided essentially the same answer.

Ref. 31. The positions of the bands, their relative intensities, and the lineshapes then were optimized by slight variations of the principal parameters of the tensors, *i.e.* $A_{x''x''}$, $A_{y''y''}$, $A_{z''z''}$, e^2qQ and η. For half-met-Ty with L-mimosine, the x'' and y'' directions of the hyperfine tensor had to be set parallel to the x' and y' directions to reduce the intensities of the bands at 0.5 and 1.0 MHz.

For all three complexes, the frequencies of the bands are nicely reproduced for most values of the magnetic field and of the time τ. The dominant nitrogen gives rise to bands at 0.5, 1.0, and 1.5 MHz and a $\Delta M_I = 2$ feature at about 4 MHz. For half-met-Ty with *p*-nitrophenol, the intensity of these bands is largest, and for half-met-Ty with L-mimosine, only the band at 1.5 MHz has significant intensity. The relative intensities of the bands also generally agree with those in the experimental spectra. The simulations can in principle be improved by further optimizing the relative orientations of the hyperfine and the quadrupole tensor, but we chose not to do so because it would lead to too many free parameters.

The optimized hyperfine and quadrupole tensors are given in Table III for the three complexes. Note that as a consequence of the nearly axial g tensor, the *x* and *y* components of the hyperfine and quadrupole principal axes are arbitrary and they are determined within a rotation around the *z*-axis. These components are included nonetheless in the table (where we chose the *x* and *y* directions about parallel to the Cu-Nϵ directions of histidines 324 and 364, respectively) to specify the relative orientation of the principal directions of the quadrupole and hyperfine tensors. For half-met-Ty, the Nδ of histidine 364 dominates the ESEEM spectrum and is characterized by the largest hyperfine coupling (A_{iso} = 1.80 MHz). The second nitrogen, that of histidine 324 (A_{iso} = 1.35 MHz), makes a minor contribution to the spectrum. When *p*-nitrophenol binds, the hyperfine coupling of the Nδ of histidine 364 increases and dominates the ESEEM spectrum to such an extent that the contribution of the Nδ of histidine 324 to the ESEEM spectrum becomes undetectable. When L-mimosine binds, the change in the ESEEM pattern is compatible with a decrease in the hyperfine coupling of the nitrogen of histidine 364 (A_{iso} = 1.50 MHz). For all cases, the values of e^2qQ and η are virtually identical to those read from the spectra.

Structural Implication for the Binding of Inhibitors—The structural model for the half-met derivative of *S. antibioticus* Ty that emerges from the analysis of the cw EPR data implies a four-coordinated cupric site, where three of the ligands are likely to be the conserved histidines. The absence of well resolved superhyperfine features from the directly coordinated nitrogens, however, does not allow us to directly "count" the copper bound nitrogens in the cw EPR spectrum. The contributions of at least two distinct remote histidyl nitrogens have been identified in the nitrogen region of the HYSCORE spectra and accordingly the contribution of two non-equivalent nitrogens has been used to obtain the best simulation to the field and τ-dependent ESEEM data. The failure to detect the contribution of the third histidine residue in the pulsed EPR experiment is probably related to the magnitude of the hyperfine interaction of its remote nitrogen that may be too far from the so-called "exact cancellation condition." Support for the presence of three ligand histidine residues is provided by the highly conserved sequences in the active site region of all proteins with a type-3 site that always show a pattern of six conserved metal ligand histidines. This pattern is present also in *S. antibioticus* Ty. More importantly, experimental evidence of coordination by three His residues for each copper ion of *S. antibioticus* Ty comes from

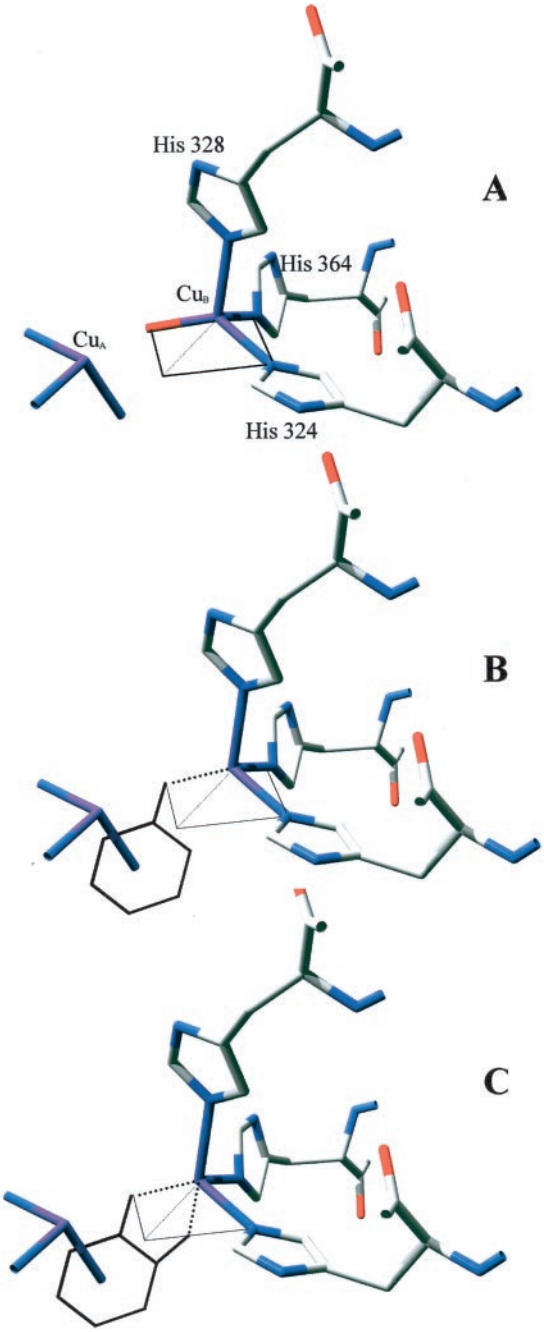

FIG. 7. **Structure of the active site of met-Hc from *L. polyphemus* (4, 5).** The structure was used as a template for the simulations of the ESEEM spectra of half-met-Ty and its inhibitor-bound complexes (see "Results"). *A*, the ligands of the paramagnetic Cu_B ion consist of the histidines 324, 328, and 364 (numbering is according to the sequence of *L. polyphemus* subunit II Hc) and a water molecule. *B*, half-met-Ty with bound *p*-nitrophenol and *C*, half-met-Ty with bound L-mimosine. The ligands of the Cu_A ion are not shown in the figure. The *red arrows* represent the z direction of the nitrogen quadrupole.

a paramagnetic NMR study (9), where the signals from a total of six Nϵ-coordinated histidines were assigned in the NMR spectra of the met [Cu(II)-OH^--Cu(II)] resting form. The Nϵ coordination for the ligand histidine fits with the parameters obtained for the hyperfine interaction of the remote nitrogen from the simulation of the ESEEM data (32).

The nature of the fourth ligand previously has been unambiguously proven by hyperfine sublevel correlation (HYSCORE) spectroscopy to be an oxygen of a water or hydroxyl group (15), which provided a means for the evaluation of the

hyperfine interaction. Its magnitude appeared to be diagnostic of an equatorial coordination of this exogenous ligand (15). The data presented in this study do not provide an indication on whether or not the second (cuprous) ion is involved in the coordination of this water molecule. What is stated above can be summarized in a structural model (Fig. 7*A*) where the paramagnetic center is on the Cu_B and the latter is tetra coordinated. The choice of Cu_B and not Cu_A as the paramagnetic center in the half-met-Ty is based on the observation that only this assignment gave consistent results in the simulation of the quadrupole data for the histidine Nδ atoms. The coordination geometry of the metal ion, however, can only tentatively be considered as tetragonally distorted.

The definition of a structural model for the half-met derivative provides a tool to investigate the interaction with different types of competitive inhibitor. The first molecule investigated was *p*-nitrophenol. The presence of a nitro substituent in the *para* position results in a very poor substrate that in the native protein acts as a competitive inhibitor of L-Dopa oxidation with an inhibition constant of 700 μM.[4] Binding to the cupric center is demonstrated by both the changes in the lineshape of the cw EPR spectrum and by the absence of the contribution from the bound water molecule in the HYSCORE spectrum of the half-met-Ty with *p*-nitrophenol (15). The virtually unchanged $g_{||}$ and $A_{||}$ values suggest that the Cu(II) remains four-coordinated and that the coordination geometry is not significantly modified upon *p*-nitrophenol binding. The binding may simply be an exchange of the bound hydroxyl moiety coordinated in the *trans* position to His-324 as indicated in Fig. 7*B*. It should be mentioned that this coordination mode for *p*-nitrophenol is more likely to be relevant for the inhibition mechanism of *p*-nitrophenol on met-Ty rather than for the binding mode of phenols in the monooxygenation reaction where the binding of the phenol substrate occurs to a Cu(II)-peroxo complex.

A more complex effect on the coordination of Cu(II) has to be assumed to rationalize the modification observed upon binding of a bidentate hydroxyquinone such as kojic acid or L-mimosine. These are among the strongest competitive inhibitors of bacterial tyrosinase with inhibition constants of 4 and 30 μM, respectively (17). In this case the disappearance of the signal of the bound water molecule in the HYSCORE spectrum upon inhibitor binding observed previously (15) is accompanied by a more significant change in the paramagnetic properties of the Cu(II) in the active site. The $g_{||}$ and $A_{||}$ values for both hydroxyquinone complexes are indicative of penta-coordination, and this can be achieved if both oxygen atoms of the inhibitors coordinate to the Cu(II) as shown in Fig. 7*C*. In agreement with the proposed binding mode for hydroxyquinones, an x-ray absorption edge study on the met-form of *N. crassa* Ty indicates a substantially distorted tetra-coordinated Cu(II) ion (33). Furthermore, the extended x-ray absorption fine structure data indicate an increase in the number of atoms in the first coordination shell of the metal ions in the active site upon binding of L-mimosine to met-Ty (33).

Indirect evidence that bidentate ligands bind with both oxygen atoms to Cu(II) is found in the analysis of the half-met-Ty complex with toluic acid. In hydroxyquinones the ligand oxygens conjugated to the aromatic ring are 2.7 Å apart, while in the carboxylic group of toluic acid the two oxygen ligands are 2.3 Å apart. The structural consequence of this difference, when assuming bidentate ligation, is a more distorted coordination geometry for the carboxylic complex than for the hydroxyquinone complex, as actually observed for the toluic acid half-met-Ty complex.

The proposed binding mode where both oxygen atoms of the hydroxyquinones bind to the Cu(II) has several important implications for the enzymatic reaction mechanism of tyrosinase. First, it does not assume a different coordination mode for mono- and bidentate molecules. This would mean that both substrates dock into the same region of the active site. The second aspect is that the proposed binding mode does not imply a structural rearrangement of the diphenol reaction intermediate when the monophenols are converted to diquinones. It is important to point out that it is not possible solely on the data presented here to exclude a role for the Cu(I) in the binding. Furthermore, no simple correlation can be made between the observed inhibition constant and the structure of the inhibitors, although in general bidentate hydroxyquinone ligands seem to bind stronger than monodentate inhibitors.

In conclusion, a transition state analogue as shown in Fig. 7*C*, which is based on the data obtained for inhibitors such as kojic acid and L-mimosine, provides a model for the binding of the diphenols that are generated as intermediates during turnover of the enzyme, when monophenols are converted into quinones (Scheme 3 in Ref. 15).

[4] L. Bubacco, M. Gastel, E. J. J. Groenen, E. Vijgenboom, and G. W. Canters, unpublished result.

REFERENCES

1. Solomon, E. I., Sundaram, U. M., and Machonkin, T. E. (1996) *Chem. Rev.* **96,** 2563–2605
2. Volbeda, A., and Hol, W. G. J. (1989) *J. Mol. Biol.* **206,** 531–546
3. Volbeda, A., and Hol, W. G. J. (1989) *J. Mol. Biol.* **209,** 249–279
4. Hazes, B., and Hol, W. G. (1992) *Proteins* **12,** 278–298
5. Hazes, B., Magnus, K. A., Bonaventura, C., Bonaventura, J., Dauter, Z., Kalk, K. H., and Hol, W. G. (1993) *Protein Sci.* **2,** 597–619
6. Magnus, K. A., Hazes, B., Ton That, H., Bonaventura, C., Bonaventura, J., and Hol, W. G. (1994) *Proteins* **19,** 302–309
7. Cuff, M. E., Miller, C., van Holde, K. E., and Hendrickson, W. A. (2000) *J. Mol. Biol.* **278,** 855–870
8. Klabunde, T., Eicken, C., Sacchettini, J. C., and Krebs, B. (1998) *Nat. Struct. Biol.* **5,** 1084–1090
9. Bubacco, L., Salgado, J., Tepper, A. W. J. W., Vijgenboom, E., and Canters, G. W. (1999) *FEBS Lett.* **442,** 215–220
10. Decker, H., and Tuczek, F. (2000) *Trends Biochem. Sci.* **25**
11. Himmelwright, R. S., Eickman, N. C., Lubien, C. D., Lerch, K., and Solomon, E. I. (1980) *J. Am. Chem. Soc.* **102,** 7339–7344
12. Wilcox, D. E., Porras, A. G., Hwang, Y. T., Lerch, K., Winkler, M. E., and Solomon, E. I. (1985) *J. Am. Chem. Soc.* **107,** 4015–4027
13. Winkler, M. E., Lerch, K., and Solomon, E. I. (1980) *J. Am. Chem. Soc.* **103,** 7001–7003
14. Decker, H., Dillinger, R., and Tuczek, F. Angew. (2000) *Chem. Int. Ed. Eng.* **39,** 1591–1595
15. van Gastel, M., Bubacco, L., Groenen, E. J. J., Vijgenboom, E., and Canters, G. W. (2000) *FEBS Lett.* **474,** 228–232
16. Katz, E., Thompson, C. J., and Hopwood, D. A. (1983) *J. Gen. Microbiol.* **129,** 2703–2714
17. Bubacco, L., Vijgenboom, E., Gobin, C., Tepper, A. W. J. W., Salgado, J., and Canters, G. W. (2000) *J. Mol. Catal. B Enzym.* **8,** 27–35
18. Jolley, R. L., Evans, L. H., Makina, N., Mason, S. (1974) *J. Biol. Chem.* **249,** 335–345
19. Jackman, M. P., Hajnal, A., and Lerch, K. (1991) *Biochem. J.* **274,** 707–713
20. Lerch, K., and Ettlinger, L. (1972) *Eur. J. Biochem.* **31,** 427–437
21. Disselhorst, J. A. J. M., van der Meer, H., Poluektov, O. G., Schmidt, J. (1995) *J. Magn. Reson. A* **115,** 183–188
22. Neese, F. (1995) *QCPE Bulletin* **15,** 5, University of Indiana, Bloomington, IN
23. van Gastel, M., Coremans, J. W. A., Jeuken, L. J. C., Canters, G. W., Groenen, E. J. J. (1998) *J. Biol. Inorg. Chem.* **102,** 4462–4470
24. Mims, W. B., Peisach, J., and Davis, J. L. (1977) *J. Chem. Phys.* **66,** 5536–5550
25. Mims, W. B., and Peisach, J. (1978) *J. Chem. Phys.* **69,** 4921–4929
26. Abragam, A., and Bleaney, B. (1970) *Electron Paramgnetic Resonance of Transition Metal Ions*, Clarendon Press, Oxford
27. Mondovi, B., Graziani, M. T., Mims, W. B., Oltzik, R., Peisach, J. (1977) *Biochemistry* **16,** 4189–4201
28. Peisach, J., and Blumberg, W. E. (1974) *Arch. Biochem. Biophys.* **165,** 691–708
29. Flanagan, H. L., and Singel, D. J. (1987) *J. Chem. Phys.* **87,** 5606–5616
30. Coremans, J. W. A., Poluektov, O. G., Groenen, E. J. J., Canters, G. W., Nar, H., Messerschmidt, A. (1996) *J. Am. Chem. Soc.* **118,** 12141–12153
31. Magliozzo, R. S., Bubacco, L., McCracken, J., Jiang, F., Beltramini, M., Salvato, B., and Peisach, J. (1995) *Biochemistry* **34,** 1513–1523
32. Jiang, F., McCracken, J., and Peisach, J. (1990) *J. Am. Chem. Soc.* **112,** 9035–9044
33. Woolery, G. L., Powers, L. S., Winkler, M., Solomon, E. I., Lerch, K., and Spiro, T. G. (1984) *Biochim. Biophys. Acta* **788,** 155–161
34. Bubacco, L., Magliozzo, R. S., Wirt, M. D., Beltramini, M., Salvato, B., Peisach, J. (1995) *Biochemistry*, **34,** 1524–1533

35. Olesen, K, Veselov, A., Zhao, Y., Wang, Y., Danner, B., Scholes, C. P., Shapleigh, J. P. (1998) *Biochemistry*, **37,** 6086–6094
36. Reinhard, H., Kappl, R., Hüttermann, J., Viezzoli, M. S. (1994) *J. Phys. Chem.* **98,** 8806–8812
37. Rosenberg, R. C., Root, C. A., Bernstein, P. K., Gray, H. B. (1975) *J. Am. Chem. Soc.*, **97,** 2092–2096
38. Kitajima, N., Fujisawa, K., Fujimoto, C., Moro-oka, Y., Hashimoto, S., Kitagawa, T., Toriumi, K., Tatsumi, K., Nakamura, A. (1992) *J. Am. Chem. Soc.*, **114,** 1277–1291
39. J. C. S.Sakaguchi, U., Addison, A. W. (1978) *J. Chem. Soc. Dalton Trans.*, 600–608
40. Bhalla, R., Helliwell, M., Garner, D. (1997) *Inorg. Chem.*, **36,** 2944–2949
41. Barta, G., Mathur, P. (1992) *Inorg. Chem.*, **31,** 1575–1580
42. Burns, C. S., Aronoff-Spencer, E., Dunham, C. M., Lario, P., Avdievich, N. I., Antholine, W. E., Olmstead, M. M., Vrielink, A., Gerfen, G. J., Peisach, J., Scott, W. G., Millhauser, G. (2002) *Biochemistry*, **41,** 3991–4001
43. Colaneri, M. J., Vitali, J., Peisach, J. (2000) *Biochemistry*, **39,** 584–591
44. Abuhijleh, A. L., Woods, C. (1993) *Inorg. Chim. Acta*, **209,** 187–193
45. Conrad, J. S., Dawso, S. R., Hubbard, E. R., Meyers, T. E., Strothkamp, K. G. (1994) *Biochemistry* **33,** 5739–5744